Joint inversion of seismic and gravity data for lunar composition and thermal state up the Moon is derived from the impactor.

A. Khan, J.A. D. Connolly, J. Maclennan, K. Mosegaard

Geophys. J. Int. (2007) **168,** 243–258 doi: 10.1111/j.1365-246X.2006.03200.x

Joint inversion of seismic and gravity data for lunar composition and thermal state

A. Khan,[1,2] J. A. D. Connolly,[3] J. Maclennan[4,5] and K. Mosegaard[1]

[1] *Niels Bohr Institute, University of Copenhagen, Denmark. E-mail: amir@gfy.ku.dk*
[2] *DGSP, Institut de Physique du Globe de Paris, France*
[3] *Earth Sciences Department, Swiss Federal Institute of Technology, Zurich, Switzerland*
[4] *School of GeoSciences, The University of Edinburgh, Grant Institute, Edinburgh, UK*
[5] *Department of Earth Sciences, University of Cambridge, Cambridge, UK*

Accepted 2006 August 23. Received 2006 August 22; in original form 2005 August 31

SUMMARY

We invert the Apollo lunar seismic data set, together with lunar mass and moment of inertia, directly for the chemical composition and thermal state of the Moon. The lunar mantle and crust are modelled in the chemical system CaO–FeO–MgO–Al_2O_3–SiO_2. The stable minerals, their seismic properties, and the bulk density are computed by Gibbs free energy minimization. Voigt–Reuss–Hill averaging is then used to compute seismic-wave velocity profiles, from which traveltimes are estimated, while mass and moment of inertia are obtained by integration of the density profile. Given this scheme, the data are jointly inverted using a Markov chain Monte Carlo algorithm, from which a range of compositions and temperatures fitting data within uncertainties are obtained. The analysis constrains the range of compositions, thermal states, mineralogy and physical structure of the lunar interior that are consistent with data. Additionally, the analysis provides estimates for the size and density of the lunar core. The inferred lunar compositions have lower Mg#s (∼83) than the Earth's mantle (∼89), suggesting that the Moon was derived from material other than the Earth's mantle. This supports giant impact simulations of lunar origin that show that more than 80 per cent of the material making up the Moon is derived from the impactor.

Key words: inversion, thermodynamic modeling, mantle composition, mantle temperature, physical structure.

1 INTRODUCTION

Of all geophysical methods used to study a planet's structure, seismology is uniquely suited to determine many of the parameters that are essential to understanding the dynamic behaviour of the planet. For this reason seismology has played a leading role in the study of the internal structure of the Earth. The only other solar system body from which we have seismic observations pertinent to its interior properties is the Moon, thus giving us an opportunity to examine planetary formation independently of the Earth. Issues that can be addressed geophysically and which hold the potential of providing constraints on lunar formation and evolution, include the question of whether the Moon has a metallic iron core, the depth of differentiation needed to produce the plagioclase rich highland crust, its bulk composition and the question whether it bears any generic relationship to that of the Earth's mantle.

From 1969 to 1972 the US Apollo program installed one short-lived and four long-lived seismometers on the Moon. The latter instruments were operated until 1977. The data collected by the Apollo seismic network provided the basis for a number of earlier studies of lunar seismicity and internal structure (e.g. Toksöz *et al.* 1974; Goins *et al.* 1981a; Nakamura *et al.* 1982). Given the much increased computer capabilities over the last 25 yr, the Apollo lunar seismic data have become the focus of renewed interest, enabling the acquisition of previously unobtainable information (Khan *et al.* 2000; Khan & Mosegaard 2002; Lognonné *et al.* 2003; Bulow *et al.* 2005; Nakamura 2005).

Seismic velocity profiles are not an end in themselves, and therefore, inversions for seismic structure can only be used as an indirect means of inferring the internal state and composition of the Moon, by, for example, comparing laboratory measurements of seismic-wave velocities made on returned samples and terrestrial analogues with those obtained from the inversions. In view of the limitations inherent in this process, we propose to infer composition and thermal state of the lunar mantle directly by a joint inversion of the Apollo lunar seismic-arrival time data set, lunar mass and moment of inertia.

From an inverse problem theoretical point of view, the inversion of seismic and gravity data presented here serves a deeper purpose than simply attempting to invert for chemical composition and thermal state. There is much to be gained by the integration of widely different data sets, where one would usually invert for a set of parameters that *a priori* do not have anything in common. For instance, inversion of seismic data give information on seismic-wave

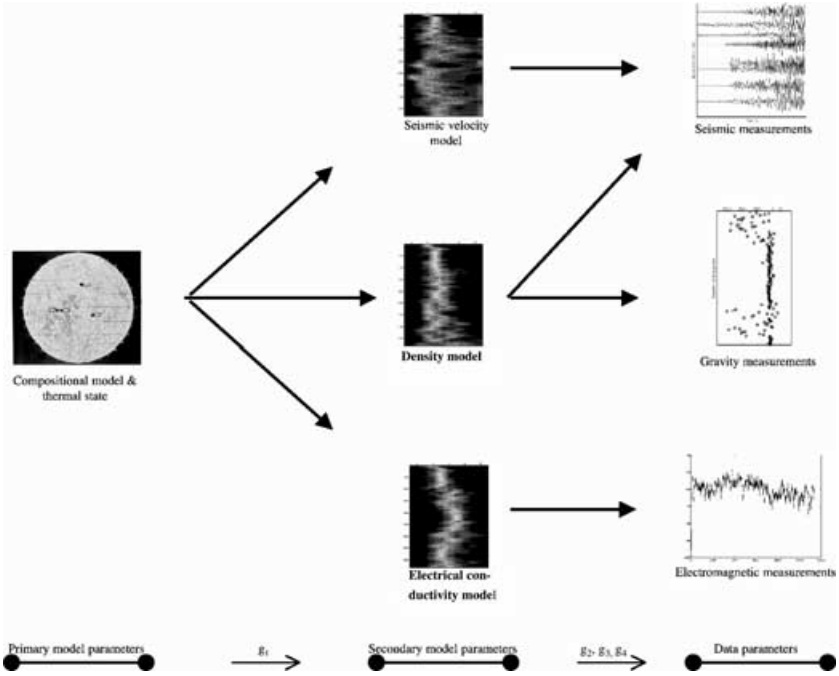

Figure 1. An illustration of the objective behind this study, termed multiparameter inversion, where the goal is to invert plural geophysical data to obtain information on a set of parameters that describes the system at a fundamental level. The different geophysical observations could, for example, be seismic-arrival times, gravity data and electromagnetic sounding data. The figure shows the different model and data parameters underlying the description of the geophysical problem as well as the different theories ($g_1, \ldots, g_4$) employed in calculating data given the composition and selenotherm.

velocities, and electromagnetic sounding data provide knowledge on the electrical conductivity profile, while gravity data tell us about the subsurface density structure. However, at this level of the inversion it is not possible to constrain, for example, seismic velocities from inversion of electromagnetic sounding data, unless, of course, laboratory measurements or physical laws are available correlating the particular parameters of interest. By appealing to a set of parameters which are not only common to all data sets, but also characterizes the media under study at a fundamental level, we present a way of integrating different geophysical data sets into a joint inversion. This is exemplified in Fig. 1. The important point to note here is that the method not only enables us to link the various geophysical data in a natural way, but that it also provides a means of introducing information on various aspects of the media, such as its mineralogy, petrology, geology and geophysics, that can equally serve to correlate the geophysical data in the inversion. The method provides a generic way of constructing planetary models where the radial variation of mineralogy, density and seismic-wave velocity with pressure and temperature are naturally specified, allowing for the direct inversion of parameters such as chemical composition, temperature, mineralogy, density and velocity structure.

Kuskov & Kronrod (1998, 2001) estimated lunar composition by inverting previously derived seismic velocity models, mass and moment of inertia in conjunction with a free energy minimization model that was used to compute the lunar mineralogy. In contrast to Kuskov & Kronrod, here we directly confront the primary seismic data and simultaneously consider gravitational data using a non-linear inversion method. The method presented here has also been extended to other planets as well as data, and includes:

(1) Inversion of electromagnetic sounding data to constrain mantle composition and thermal state of the Earth and the Moon (Khan *et al.* 2006a,b).

(2) Inversion of geophysical data pertinent to the interior of Mars (Khan & Connolly 2006).

Previous terrestrial studies encompassed only certain aspects of what is undertaken here (e.g. Goes *et al.* 2000; Cammarano *et al.* 2003; Deschamps & Trampert 2004; Godey *et al.* 2004; Shapiro & Ritzwoller 2004; Trampert *et al.* 2004; Mattern *et al.* 2005).

As the inversion of seismic traveltimes, mass and moment of inertia for composition, thermal state and other parameters is strongly non-linear, the inverse problem is formulated within the Bayesian framework. This involves the use of probability density functions (*pdf*'s) to delineate the various states of information of the problem. (Tarantola & Valette 1982; Tarantola 2004). The solution to the inverse problem is defined as the conjunction of these *pdf*'s and contained in the posterior *pdf*, from which samples are obtained by employing a Markov chain Monte Carlo (MCMC) method (e.g. Mosegaard & Tarantola 1995).

In the following sections, we present the basic theory for jointly inverting different geophysical fields, while subsequent sections detail the application to the specific problem of jointly inverting Apollo lunar seismic and gravity data for lunar composition and thermal state. As concerns the content of this paper, it is primarily concerned with methodology. Interpretation and comparison of the results to earlier lunar investigations as well as implications of these for lunar origin and evolution are described in Khan *et al.* (2006d).

2 THE INVERSE PROBLEM—GENERAL FORMULATION

2.1 Statement and solution of the inverse problem

The present approach to solving the inverse problem will be within the Bayesian framework using *pdf*'s. The solution is contained in the posterior probability density and is obtained by a con-

junction of the available information (e.g. Tarantola & Valette 1982). Samples from this posterior distribution are then obtained by employing a MCMC method as described in Mosegaard & Tarantola (1995).

Any information we have about the model $\mathbf{m}$ obtained independently of data is contained in the prior *pdf* $\eta(\mathbf{m})$. When knowledge about data as well as the physical theory linking the unknown model to data is taken into account (described by the likelihood function $\mathcal{L}(\mathbf{m})$), we update the prior to the posterior *pdf* $\sigma(\mathbf{m})$, which constitutes the solution to our problem (Tarantola & Valette 1982)

$$\sigma(\mathbf{m}) = k\eta(\mathbf{m})\mathcal{L}(\mathbf{m}), \tag{1}$$

where k is a normalization constant. As regards the functional form of the likelihood function, it is determined by the observations and the type of uncertainties used in describing data noise as well as the errors connected with the physical modelling (if quantifiable). If, as in our case, we are considering several independent geophysical observations, the likelihood function can be written as the product of a number of likelihood functions pertaining to the individual geophysical data,

$$\mathcal{L}(\mathbf{m}) = \prod_{\alpha} \mathcal{L}_{\alpha}(\mathbf{m}), \tag{2}$$

where $\mathcal{L}_{\alpha}(\mathbf{m})$ is the likelihood function for every independent geophysical method considered.

Since we, in the present interdisciplinary context, are dealing with various data sets that are a manifestation of different unrelated properties when described by parameters at the geophysical level, but of the same properties at the more fundamental level of chemistry, an extension of the above theory along the lines of Bosch (1999) is called for.

2.2 The joint posterior distribution

Estimating different media properties from the joint inversion of several *a priori* unrelated geophysical data sets, is exemplified in a very thorough analysis by Bosch (1999). He makes the distinction between primary (lithology) and secondary (seismic-wave velocities, magnetic susceptibility) parameters to jointly invert airborne measurements of magnetic and gravity data for subsurface lithology over a 2-D model. This division into primary and secondary model parameters, as shown in Fig. 1, therefore, prompts the following extension of eq. (1) to the case where we consider a joint model parameter space $\mathcal{M}$ as the product of two model spaces $\mathcal{M}_p \times \mathcal{M}_s$ (this is easily generalized to the case of n model parameter spaces). $\mathcal{M}_p$ and $\mathcal{M}_s$ are called primary and secondary model parameter spaces, respectively, and contain primary and secondary model parameter arrays, $\mathbf{m}_p$ and $\mathbf{m}_s$. In the joint model space $\mathcal{M}$, we obviously have $\mathbf{m} = \{\mathbf{m}_p, \mathbf{m}_s\}$. Let us furthermore imagine having performed a number of different geophysical measurements, each leading to a data parameter vector $\mathbf{d}_1, \mathbf{d}_2, \ldots, \mathbf{d}_k$ defined in the data spaces $\mathcal{D}_1, \mathcal{D}_2, \ldots, \mathcal{D}_k$. In the joint data parameter space $\mathcal{D} = \mathcal{D}_1 \times \mathcal{D}_2 \times \cdots \times \mathcal{D}_k$), we can write the joint data parameter array as $\mathbf{d} = \{\mathbf{d}_1, \mathbf{d}_2, \ldots, \mathbf{d}_k\}$. Our problem now consists of inferring information on $\mathbf{m}_p$ and $\mathbf{m}_s$ from the k data parameter vectors and whatever prior information available. The posterior distribution, eq. (1), in the joint model space can be written as

$$\sigma(\mathbf{m}_s, \mathbf{m}_p) = k\eta(\mathbf{m}_s, \mathbf{m}_p)\mathcal{L}(\mathbf{m}_s, \mathbf{m}_p). \tag{3}$$

Since we are dealing with two model parameter sets where the secondary parameters are derived from the primary model parameters, and therefore depend on these, we can decompose the prior *pdf* into two parts by using conditional probabilities (any *pdf* can be written this way)

$$\eta(\mathbf{m}_s, \mathbf{m}_p) = \eta_s(\mathbf{m}_s \mid \mathbf{m}_p)\eta_p(\mathbf{m}_p), \tag{4}$$

where $\eta_p(\mathbf{m}_p)$ represents a marginal prior *pdf* in the primary model space and contains information on primary model parameters only. $\eta_s(\mathbf{m}_s \mid \mathbf{m}_p)$ is a conditional *pdf* in the secondary model parameter space and it describes prior knowledge on $\mathbf{m}_s$ as well as the dependence of $\mathbf{m}_s$ on $\mathbf{m}_p$.

Given that the physical law in going from $\mathbf{m}_p$ to $\mathbf{m}_s$ is different from the one used to perform the step $\mathbf{m}_s \rightarrow \mathbf{d}$, we can decompose the likelihood function in much the same way as we treated the prior *pdf*. Let us assume that $\mathcal{L}(\mathbf{m})$ has been normalized and write it as $\hat{\mathcal{L}}(\mathbf{m})$. This permits the following decomposition

$$\begin{aligned} \hat{\mathcal{L}}(\mathbf{m}_s, \mathbf{m}_p) &= \mathbf{c}\mathcal{L}(\mathbf{m}_s, \mathbf{m}_p), \\ \hat{\mathcal{L}}(\mathbf{m}_s, \mathbf{m}_p) &= \mathbf{c}\mathcal{L}_s(\mathbf{m}_s \mid \mathbf{m}_p)\mathcal{L}_p(\mathbf{m}_p), \end{aligned} \tag{5}$$

where c is a normalization constant. $\mathcal{L}_p(\mathbf{m}_p)$ is the likelihood function that calculates secondary model parameters given values of primary model parameters and $\mathcal{L}_s(\mathbf{m}_s \mid \mathbf{m}_p)$ is another likelihood function that calculates data given values of $\mathbf{m}_s$, conditional on $\mathbf{m}_p$. By substituting the expressions for the prior *pdf* and the likelihood function, eqs (4) and (5), into eq. (3), the posterior distribution can be written as

$$\sigma(\mathbf{m}_s, \mathbf{m}_p) = \mathrm{k}\eta_s(\mathbf{m}_s \mid \mathbf{m}_p)\eta_p(\mathbf{m}_p)\mathcal{L}_s(\mathbf{m}_s \mid \mathbf{m}_p)\mathcal{L}_p(\mathbf{m}_p), \tag{6}$$

where $\mathsf{k}=\mathsf{c}k$. By re-arranging terms and employing $\mathrm{k} = \mathrm{k}_1\mathrm{k}_2$ we obtain

$$\begin{aligned} \sigma(\mathbf{m}_s, \mathbf{m}_p) &= \mathrm{k}_2\eta_s(\mathbf{m}_s \mid \mathbf{m}_p)\mathcal{L}_s(\mathbf{m}_s \mid \mathbf{m}_p)\mathrm{k}_1\eta_p(\mathbf{m}_p)\mathcal{L}_p(\mathbf{m}_p) \\ &= \sigma_s(\mathbf{m}_s \mid \mathbf{m}_p)\sigma_p(\mathbf{m}_p), \end{aligned} \tag{7}$$

which shows that the posterior *pdf* in the joint model space is given by the product of the posterior *pdf*'s defined in the model spaces $\mathcal{M}_p$ and $\mathcal{M}_s$. In Section 3.3 we will deal specifically with the individual *pdf*'s η_p, η_s, $\mathcal{L}_p$ and $\mathcal{L}_s$, when applying the theory to the simultaneous inversion of seismic and gravity data.

2.3 Sampling the joint posterior distribution

Having defined the posterior distribution above (eq. 7), as the solution to our inverse problem containing all the information about our model $\mathbf{m}$ from data $\mathbf{d}$ and prior information, the question that arises next is how to extract the information from the posterior distribution. To generally characterize our model, we need to compute summary properties of the posterior *pdf*. Of usual interest are marginal distributions of selected parameters in $\mathbf{m}$, providing us with, for example, the uncertainty on the parameter of interest. In the case of the general inverse problem, however, the posterior *pdf* does not exist as an analytical function and given its usually complex shape defined over a high-dimensional model space it can not be integrated analytically. Instead we have to estimate posterior probabilities by statistical integration methods which consist of approximating the *pdf* integral by a summation over a sample from the posterior distribution (e.g. Mosegaard 1998)

$$\int_{\Lambda} f(\mathbf{m})\sigma(\mathbf{m})d\mathbf{m} \approx \frac{1}{N} \sum_{\{n \mid \mathbf{m}_n \in \Lambda\}} f(\mathbf{m}_n), \tag{8}$$

where Λ is an event or a subset of the model space, $n = 1, \ldots, N$ the position in the chain of N sampled models and f an indicator function, given by

$$f(\mathbf{m}) = \begin{cases} 1, & \text{if } \mathbf{m} \in \Lambda \\ 0, & \text{if } \mathbf{m} \notin \Lambda. \end{cases} \tag{9}$$

From this expression any desired characteristic of the posterior *pdf*, such as marginal or conditional probabilities or others, like means and variances of model parameters, can easily be evaluated, essentially performing an integration. MCMC algorithms have been found to be extremely well adapted for Bayesian inference problems. This is especially true in cases where $\eta(\mathbf{m})$ and $\mathcal{L}(\mathbf{m})$ are complicated functions and where the evaluation of the likelihood functions involves solving non-linear forward model operators, which usually do not exist in closed analytical form, but rather as computer-intensive algorithms (e.g. Mosegaard & Tarantola 1995). The main idea is, therefore, to design a random walk in the model space which samples the posterior probability density, that is, samples models that are consistent with data and prior information and where the choice of the next state (i.e. next model) depends only upon the current state. The random walk is generally said to be independent of the starting model and will after a number of moves (termed the 'burn-in' period), converge on a region of high posterior probability. Once convergence has been reached, the retaining of samples commences and it can be shown that this chain of models can be made to sample any desired *pdf*, that is, it can be designed to sample models distributed according to the posterior *pdf* (e.g. Gelfand & Smith 1990; Gelman & Rubin 1992; Tierney 1994; Besag *et al.* 1995). The versatility of the MCMC method is one of the reasons why it has gained in popularity (the reviews of Mosegaard & Sambridge 2002 and Sambridge & Mosegaard 2002 contain a nice compilation of various applications of MCMC methods to geophysics).

The MCMC algorithm employed here, known as the Metropolis-Hastings algorithm (Metropolis *et al.* 1953; Hastings 1970), is contained in the following rules

(1) Consider $\mathbf{m} = \{\mathbf{m}_s, \mathbf{m}_p\}$ to be some current model in the Markov chain and randomly modify it to some candidate model $\mathbf{m}' = \{\mathbf{m}'_s, \mathbf{m}'_p\}$, where the candidate model is drawn from the prior using a proposal distribution.

(2) Acceptance of $\mathbf{m}'$ is governed by the probability

$$\mathcal{P} = \min\left[1, \frac{\mathcal{L}(\mathbf{m}')}{\mathcal{L}(\mathbf{m})}\right] \tag{10}$$

If $\mathbf{m}'$ is accepted then it becomes the current model, otherwise the current state remains $\mathbf{m}$. A factor of great importance, especially when we are concerned with high-dimensional spaces, where a large proportion of the volume may have near-zero probability density, is that this algorithm renders us capable of sampling the space with a sampling density proportional to the given probability density without excessively sampling low-probability areas of the model space.

3 APPLICATION TO THE JOINT INVERSION OF LUNAR SEISMIC AND GRAVITY DATA

3.1 Geophysical data

The lunar seismic network spans the near face of the moon in an approximate equilateral triangle with 1100 km spacing between stations, with two seismometers placed 180 km apart at one corner and covers most geological settings on the front side of the Moon. Since the first mission more than 12 000 events have been recorded and catalogued (Nakamura *et al.* 2005). Since the compilation of the recorded seismograms, it has been shown that the Moon is aseismic compared to the Earth. In comparison to the Earth the energy released in seismic activity is eight orders of magnitude less, being about 10^{10} J yr^{-1}, compared to 10^{18} J yr^{-1} by earthquakes (Goins *et al.* 1981a), although Nakamura (1980) has pointed out that the actual average lunar seismic energy release could be as high as 10^{14} J yr^{-1}. Most of the moonquakes are small on the Richter scale with magnitudes ranging up to 4 for shallow events (Nakamura *et al.* 1974a) whereas the deep events were generally of magnitude <2 (Goins *et al.* 1981a). Because of the high sensitivity of the seismometers and the low level of microseismic background noise, however, each station detected on the average between 650 and 1250 moonquakes per year.

Upon examination of the first lunar seismic data returned to Earth in 1969, it became evident that their interpretation would be a somewhat more intricate process, due to an apparent complexity inherent in lunar seismograms. It turned out that the lunar seismic signals were characterized by being long, of high frequency and of reverberating nature with small first arrivals and slowly building amplitudes. These particular characteristics, almost ubiquitous to lunar seismic signals are thought to be due to near-surface scattering and the low level of attenuation in the crust (Latham *et al.* 1970). Unlike the Earth, where seismic pulses in general are of rather short duration, the most prominent feature of lunar signals is their anomalous long continuance. Strong signals, as those from the impacts of the upper stage of the Saturn rocket last several hours. Moonquake and meteoroid impact signals typically continue for 30 min to 2 hr.

Four distinct types of events have been identified. They are: deep moonquakes, shallow moonquakes and thermal moonquakes, all of which reflect the present dynamic state of the lunar interior, and of course meteoroid impacts. For a summary of the catalogued events detected with the long-period seismo-meters during the operation of the network see (Nakamura *et al.* 1981, 2005). For further details the reader is referred to, for example, Latham *et al.* (1969), Toksöz (1974), Toksöz *et al.* (1974) and Nakamura *et al.* (1980, 1982).

Geophysical data considered here include seismic traveltimes as well as planetary mass and moment of inertia. Because of the strong coda anything arriving after the first incoming *P* and *S* waves is essentially obscured and we are limited to inverting first arrivals only. However, even the mere picking of first arrivals is at times a difficult task, as is evidenced in the compilation by Nakamura (1983) of arrival time picks performed by several different groups. As there is no simple solution to the problem of minimizing subjectivity, we have presently chosen to focus attention on the data set obtained by Lognonné *et al.* (2003). Specifically, the geophysical data used here are lunar seismic traveltimes from a number of diverse events, including eight artificial impacts, 19 meteoroid impacts, eight shallow moonquakes and 24 deep moonquakes, registered at the four Apollo lunar seismic stations. The 59 events resulted in a total of 318 first *P*- and *S*-wave arrivals which are used in the present inversion (the arrival time picks and associated uncertainties are tabulated in Lognonné *et al.* 2003).

The other geophysical data used are lunar mass and moment of inertia. The adopted values are $M = 7.3477 \pm 0.011 \cdot 10^{22}$ kg and $I/MR^2 = 0.3935 \pm 0.0002$, based on the moment of inertia value of 0.3931 obtained through the analysis of Lunar Prospector (Konopliv *et al.* 1998) and rescaled to a mean radius of 1737.1 km (Smith *et al.* 1997).

3.2 Constructing the forward model

Solving the forward problem is generally condensed into the following statement

$$\mathbf{d} = \mathrm{g}(\mathbf{m}), \tag{11}$$

Table 1. Solution notation, formulae and model sources. Unless otherwise noted, the compositional variables x and y may vary between zero and unity and are determined as a function of the computational variables by free-energy minimization.

Symbol	Solution	Formula	Source
Crd	Cordierite	$[Mg_xFe_{1-x}]_2Al_4Si_5O_{18}$	Ideal
Cpx	Clinopyroxene	$CaMg_xFe_{1-x}Si_2O_6$	Holland & Powell (1996)
Gt	Garnet	$[Fe_xCa_yMg_{1-x-y}]_3Al_2Si_3O_{12}$, $x + y \leq 1$	Holland & Powell (1998)
Ol	Olivine	$[Mg_xFe_{1-x}]_2SiO_4$	Holland & Powell (1998)
Opx	Orthopyroxene	$[Mg_xFe_{1-x}]_{2-y}Al_{2y}Si_{2-y}O_6$	Holland & Powell (1996)
Sp	Spinel	$Mg_xFe_{1-x}Al_2O_3$	Ideal

where g is a functional relation governing the physical laws that relate model and data, expressing our mathematical model of the physical system under study. Let us look at somewhat more detail at the forward models, by splitting eq. (11) up into a number of sequences along the lines of Fig. 1

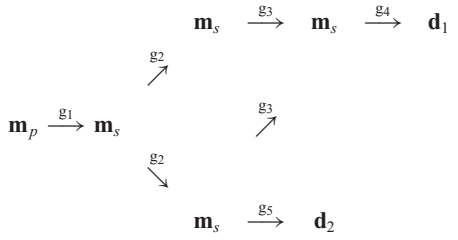

Here $\mathbf{m}_p$ is a model of an assumed starting composition, temperature profile, crust and mantle thickness. g_1 is the forward operator embodying the Gibbs free energy minimization routine, calculating mineral phase proportions (modal mineralogies) and contained in $\mathbf{m}_s$ (all subsequent parameters are assembled in $\mathbf{m}_s$). g_2 calculates physical properties using an appropriate averaging scheme. g_3 calculates seismic velocities and g_4 estimates seismic traveltimes ($\mathbf{d}_1$) using the latter parameters, while g_5 calculates mass and moment of inertia ($\mathbf{d}_2$) from the obtained densities. Some general comments about the physical model of the Moon are appropriate before describing the forward models.

Our model of the Moon is assumed to be spherically symmetric and divided into three concentric shells which are variable in size. The three layers correspond to crust, mantle and core. Crust and mantle are described by the following set of primary model parameters, its thickness d, temperature T and compositional parameter c, that specifies their compositions in the CaO–FeO–MgO–Al_2O_3–SiO_2 (CFMAS) system. Because we lack the thermodynamic data necessary to model the lunar core, the core is specified by its size and density. This simplification has no influence on the seismic inversion, as the core properties only affect the gravitational response of the moon. In the inversion, the radial node representing the core–mantle boundary (CMB) is located at 1337 km depth; however, the physical extent of the CMB is effectively variable, in the sense that the radius is not restricted to be 400 km (see Section 3.3.1 for a description of prior information). As concerns the temperature T, it is defined at six fixed radial nodes (at depths of 0, 200, 400, 500, 1000 and 1700 km). In order to determine the mineralogical structure and physical properties it also necessary to specify the pressure profile in addition to composition and temperature.

3.2.1 Petrological modelling and computation of seismic velocities

Lunar compositions were explored within the system CFMAS; a chemical model that is thought to account for more than 98 per cent of the Moon's mass (e.g. Kuskov & Kronrod 1998). While more complex treatments are possible, such as incorporating Na_2O and TiO_2 (Kuskov *et al.* 2002), we consider that the error in assessing the solution behaviour of minor oxides outweighs the descriptive benefit of including them. Cr_2O_3, NiO and MnO are likewise neglected here.

The lunar mineralogy is assumed to be dictated by equilibrium and is computed from thermodynamic data for a given model pressure, temperature and bulk composition by Gibbs energy minimization as outlined in Connolly (2005). These calculations were made taking into consideration the non-stoichiometric phases summarized in Table 1 and the stoichiometric phases and species in the thermodynamic data compilation of Holland & Powell (1998, revised 2002). The equilibrium assumption is dubious at low temperature (e.g. Rubie & Thompson 1985). In recognition of this limitation, if a model required a mineralogy at a temperature below 1073 K, then the equilibrium mineralogy was calculated at 1073 K. Thermodynamic properties, including elastic moduli, were then computed for mineralogy so obtained at the temperature of interest. This 1073 K threshold temperature is somewhat arbitrary, but consistent with experimental observations that equilibration in anhydrous silicate systems ceases at temperatures in the range 973–1173 K (Wood & Holloway 984).

Seismic velocities were computed as described in Connolly & Kerrick (2002) using the shear modulus data base summarized by Connolly (2005). Bulk aggregate elastic moduli were computed as the Voigt–Reuss–Hill average of the elastic moduli of the stable minerals under the assumption that textural anisotropy is negligible (Watt *et al.* 1976).

The physicochemical properties of interest were computed at 31 fixed radial points with specified composition and temperature (this number was found to provide more than adequate resolution for the present purposes) starting from the surface and continuing down to the CMB. The thickness of the individual layers was chosen in such a way that the highest resolution, that is, thin layers, were placed in the crust, with layer thickness increasing at the expense of resolution as we go down through the mantle.

3.2.2 Ray tracing

Once the mineral seismic *P*- and *S*-wave velocities have been estimated we use these to calculate traveltimes for the corresponding waves, emanating from a number of sources and travelling to a set of receiving stations. Given that v_P, v_S and ρ are determined at 31 fixed nodal points, our model of the Moon is partitioned into 31 layers of fixed size with each layer delineated by its physical extent (defined as the difference between the radial position of two subsequent layers boundaries), *P*- and *S*-wave velocity as determined by the thermodynamic forward modelling routines. To each shell is assigned a piecewise linearly varying *P*- and *S*-wave velocity of the form $v(r) = v_o + k \cdot r$, which is continuous at layer

boundaries and v_o and k are constants. As a result of the planet-wide impacts associated with the sweep-up of the debris from which the Moon coalesced, actual physical cracks (porosity) were produced in the surficial layers, which are believed to extent down to depths of 15–20 km (Toksöz *et al.* 1974). The presence of porosity acts to reduce seismic-wave velocities, as measurements on chondrites and lunar samples have shown (Kanamori *et al.* 1970; Yomogida & Matsui 1983). Seismic velocities in the uppermost first kilometre on the Moon have likewise been found to be low (Kovach & Watkins 1973; Cooper & Kovach 1974). To take this into account, we introduced porosity in the first four layers (corresponding to a depth of 34 km), in the form of a scalar λ_v that can take on a value from 0 to 1, with 1 corresponding to no porosity and values <1 to increased porosity. Typical porosity values in ordinary chondrites have been measured to be less than 20 per cent (Yomogida & Matsui 1983; Hons & Hildebrand 2004). Recent measurements of the effects of porosity on the elastic parameters have shown that *P*-wave velocity to first order is linearly dependent on porosity (Hons & Hildebrand 2004). The velocity in these layers is, therefore, written as $\lambda_v v$, where v is either *P* or *S*-wave velocity and $\lambda_v \in [0; 1]$ is porosity.

3.2.3 Mass and moment of inertia

Once the mineral densities as a function of depth have been calculated we can estimate lunar mass and moment of inertia using the simple relations

$$I = \frac{8\pi}{3} \int \rho(r) r^4 dr, \qquad M = 4\pi \int \rho(r)\, r^2\, dr \tag{12}$$

3.3 Solving the inverse problem

We stated the solution to our inverse problem as a conjunction of two *pdf*'s, namely prior information $\eta(\mathbf{m}_s, \mathbf{m}_p)$ and the likelihood function $\mathcal{L}(\mathbf{m}_s, \mathbf{m}_p)$. Let us specify the information comprised in the former.

3.3.1 Sampling the prior distribution

Prior information regarding primary model parameters is summarized in Table 2 below. This is the body of information contained in the marginal prior *pdf* $\eta_p(\mathbf{m}_p)$ and primary model parameters will be distributed according to this *pdf* when sampling the primary model space.

Having sampled the primary model parameters we can estimate, using the thermodynamic forward modelling routine, secondary model parameters, which include modal mineralogies $\mathcal{F}_\alpha$ (α is the number of minerals) and bulk physical properties v_P, v_S and ρ as a function of depth. Prior information concerning these parameters is summarized in Table 3 and comprises the information contained in the conditional *pdf* $\eta_s(\mathbf{m}_s \mid \mathbf{m}_p)$

In completing the construction of our joint model parameter vector, we have to add the remaining parameters, which are porosity, core density, core size and finally hypo- and epicentre coordinates of the various seismic events, in order to relocate these. We include these remaining model parameters in $\mathbf{m}_p$. It should be noted that there is no conflict in doing so, since the values of the secondary parameters are entirely independent of any parameters other than the composition in the CFMAS system, the temperature and the thickness of the crust and mantle. Prior information as concerns the remaining model parameters is given in Table 4.

We can thus summarize our primary and secondary model parameter vectors as $\mathbf{m}_p = \{d_i, c'_{ij}, T'_k, \lambda^m_v, r_{core}, \rho_{core}, Z_p, \theta_p, \phi_p\}$ and $\mathbf{m}_s = \{\mathcal{F}_{\alpha l}, v^l_P, v^l_S, \rho^l\}$, with primes above parameters denoting logarithmic parameters.

3.3.2 Sampling the posterior distribution

Having sampled prior information, the posterior distribution, is, by eq. (1) or (7), obtained by combining the former with the likelihood function $\mathcal{L}(\mathbf{m})$, that is, by taking data into account. Let us assume that the observational uncertainties and calculation errors are independent among the different geophysical methods employed. We additionally make the assumption that data uncertainties can be

Table 2. Prior information on primary model parameters.

Parameter	Description	Number	Distribution	Interval	Constraints
T	Temperature	6	log-uniform	$T_k \in [T_{k-1}; T_{k+1}]$	Temperature profiles have to satisfy the sequence $\ldots T_{k-1} \leq T_k \leq T_{k+1} \ldots$ In any given layer k, $T_k < T^p_k$, where T^p_k is the peridotite solidus of Hirschmann (2000). $T_{surface} = 0^\circ$C.
d	Compositional layer thickness	2	Uniform	$d_{crust} \in$ [30;60 km] $d_M \in [d_{crust}; d_{\mathrm{CMB}}]$ (M = mantle, and CMB = core–mantle boundary).	Radius of lunar surface is anchored at 1737 km.
c	CFMAS composition	10	log-uniform	In the mantle layer $c(\mathrm{CaO}, \mathrm{Al_2O_3}) \in$ [1;8], $c(\mathrm{FeO}) \in$ [5;20], $c(\mathrm{MgO}) \in$ [20;55] and $c(\mathrm{SiO_2}) \in$ [20;55] (all values in wt. per cent).	For the crust the concentration of the five oxides, are varied by 5 wt. per cent around the Taylor model (see Table 5).

Table 3. Prior information on secondary model parameters.

Parameter	Description	#	Distribution	Constraints
$\mathcal{F}$	Modal mineralogies	$31 \times \alpha$	Conditioned on primary model parameters	None $\alpha = 40$
ρ	Density	31	Conditioned on primary model parameters	In sampling density profiles, a penalty function has been introduced such that the algorithm is less likely to accept density models with a density decrease.
v_P	*P*-wave velocity	31	Conditioned on primary model parameters	None
v_S	*S*-wave velocity	31	Conditioned on primary model parameters	None

Table 4. Prior information on additional primary model parameters.

Parameter	Description	Number	Distribution	Interval
λ_v	Porosity (velocity)	4	Uniform	Layer 1: $\lambda_v = \lambda_v^{\mathrm{o}} + \delta_v(2\alpha - 1)$, $\lambda_v^{\mathrm{o}} = 0.6$, $\delta_v = 0.1$ and α is a uniformly distributed random number in the interval [0; 1]. Layer 2–4: $\lambda_v(i) = \lambda_v' \, \alpha(1 - \lambda_v') + \beta_i(1 - [\lambda_v' + \alpha - \alpha\lambda_v'])$, $\lambda_v' = 0.75$ and $\beta_i = i/4$.
ρ_{core}	Core density	1	Uniform	$\rho_{core} \in [\rho_m; \rho_c]$ ρ_m is the value of ρ at the base of the mantle, as estimated by VERTEX and $\rho_c = 7.5$ g cm^{-3}.
r_{core}	Core radius	1	Uniform	$r_{\mathrm{core}} \in [0; 400\,\mathrm{km}]$
Z	Depth of deep and shallow moonquakes	32	Uniform	$Z \in [0; 1737\,\mathrm{km}]$
θ, ϕ	Epicentral coordinates of seismic events (latitude, longitude)	102	Uniform	Over the entire sphere

modelled using an l_1-norm. With these specifications, the likelihood function takes the form

$$\mathcal{L}(\mathbf{m}) \propto \exp\left(- \frac{\left|d^I_{\mathrm{obs}} - d^I_{\mathrm{cal}}(\mathbf{m})\right|}{\sigma_I} - \frac{\left|d^M_{\mathrm{obs}} - d^M_{\mathrm{cal}}(\mathbf{m})\right|}{\sigma_M} - \sum_i \frac{\left|d^{P_i}_{\mathrm{obs}} - d^{P_i}_{\mathrm{cal}}(\mathbf{m})\right|}{\sigma_{P_i}} - \sum_j \frac{\left|d^{S_j}_{\mathrm{obs}} - d^{S_j}_{\mathrm{cal}}(\mathbf{m})\right|}{\sigma_{S_j}} \right), \tag{13}$$

where d_{obs} denotes observed data, $d_{\mathrm{cal}}(\mathbf{m})$ synthetic data computed using model $\mathbf{m}$ with superscripts alluding to the particular geophysical observations and σ the uncertainty on either of these. Note that uncertainties on individual arrival time readings are different.

To initiate the sampling algorithm we need some arbitrary model as the MCMC algorithm, in principle, is independent of where it starts off in the model space. However, given the complexity of the problem, we chose to start off with a model that, *a priori*, is believed to resemble the bulk composition of the Moon to some degree. For crust and mantle layers we assume the crust and bulk Moon compositions as estimated by Taylor (1982), respectively (see Table 5). To sample the posterior distribution we have to proceed along the steps outlined earlier in our description of the Metropolis-Hastings algorithm. Let us write it down for the following sequence (though simplified, this sequence is the same as the one following eq. 11)

Table 5. Bulk composition models of the silicate part of the Moon and Earth.

Model	CaO	FeO	MgO	Al_2O_3	SiO_2
Moon					
Taylor crustal model (1982)	16.5	6.5	7.0	25.0	45.5
Taylor bulk model (1982)	4.6	13.1	32.3	6.1	43.9
Warren (2005)	3.0	9.1	35.6	3.8	46.2
Kuskov & Kronrod I (1998)	4.8	10.4	28.5	6.3	50.0
Kuskov & Kronrod II (1998)	4.3	11.7	29.6	5.9	48.5
Earth					
McDonough & Sun (1995)	3.6	8.2	38.2	4.5	45.5

$$\mathbf{m}_p \xrightarrow{\mathbf{m}_p} \mathbf{m}'_p \xrightarrow{g_1,g_2,g_3} \mathbf{m}_s \xrightarrow{\mathbf{m}_s} \mathbf{m}'_s \xrightarrow{g_4,g_5} \mathbf{d}$$

by breaking it down into its constituent parts and considering these individually:

(1) $\mathbf{m}_p \xrightarrow{\mathbf{m}_p} \mathbf{m}'_p$ – prior sampling of primary model parameters in $\mathcal{M}_p$ using marginal prior η_1.

– Choose a compositional layer at random.

– Perturb its thickness at random.

– Change the composition in the system CFMAS randomly in this layer.

– Select at random one of the six layers where the temperature is defined.

– Perturb the value of the temperature in the layer.

– Complete construction of $\mathbf{m}'_\mathbf{p}$ by sampling candidate values for the remaining primary parameters (epi- and hypocentre coordinates, porosity, core density and radius) from the proposal (= prior) *pdf*.

(2) $\mathbf{m}'_p \xrightarrow{g_1,g_2,g_3} \mathbf{m}_s$ – estimation of secondary model parameters given values of primary model parameters using the forward modelling operators g_1, g_2 and g_3.

– Construct v_P, v_S and ρ model by running the thermodynamic forward model.

(3) $\mathbf{m}_s \xrightarrow{\mathbf{m}_s} \mathbf{m}'_s$ – prior sampling of secondary model parameters in $\mathcal{M}_s$ using conditional prior η_2.

– Verify that the proposed ρ model satisfies the sequence $\ldots \rho_{l-1} \leq \rho_l \leq \rho_{l+1} \ldots$.

(4) $\mathbf{m}'_s \xrightarrow{g_4,g_5} \{\mathbf{d}_1, \mathbf{d}_2\}$ – Calculation of data in the joint data parameter space $\mathcal{D}$ given proposed joint model parameter vector $\mathbf{m}' = \{\mathbf{m}'_\mathrm{s}, \mathbf{m}'_\mathrm{p}\}$ in the joint model space $\mathcal{M}$ using the forward modelling operators g_4 and g_5.

– Calculate traveltimes as well as lunar mass and moment of inertia by running the ray tracer and the mass and moment of inertia calculations.

(5) Acceptance or rejection of proposed model.

– Compute acceptance probability $\mathcal{P}$ using the expression

$$\mathcal{P} = \min\left[1, \frac{\mathcal{L}(\mathbf{m}')}{\mathcal{L}(\mathbf{m})}\right]$$

– Select a random number $\alpha \in [0; 1]$ and compare it to $\mathcal{P}$. Accept $\mathbf{m}' = \{\mathbf{m}'_\mathrm{s}, \mathbf{m}'_\mathrm{p}\}$ if $\alpha < \mathcal{P}$, otherwise leave $\mathbf{m} = \{\mathbf{m}_s, \mathbf{m}_p\}$ unchanged.

(6) Return to step 1.

This sequence of steps will produce samples which are distributed according to the posterior *pdf* (Mosegaard & Tarantola 1995). The final collection of samples, then, constitutes our output, which can be used to infer the interior composition and structure of the Moon.

Convergence is reached after roughly 1000 iterations. Only after convergence had been reached, and sampled models fit the observations, did we retain samples from the posterior *pdf*. As a practical criterion to ensure convergence of the MCMC algorithm, we monitored the time-series of all output parameters from the algorithm to verify that these were indeed stationary over the many iterations performed. The question as to how many samples are needed to adequately represent the posterior *pdf*, is assumed answered once there are no longer any significant changes to the characteristics of the posterior *pdf*. To further ensure that we have adequately sampled the model space and to verify that the algorithm is actually independent of the starting model we also chose to recommence the algorithm at a number of different places in the model space, corresponding to different starting models. As to the issue of obtaining independent samples, the way that we dealt with this problem was to introduce an 'elapse time' (number of iterations) between retention of samples, which was found to be 100 by analysing the autocorrelation function of the fluctuations of the likelihood function. In all 1.2 million models have been sampled from which 12 000 were kept for further analysis, with an overall acceptance rate of ∼40 per cent.

4 ANALYSIS AND VISUALIZATION OF POSTERIOR RESULTS

The posterior probabilities calculated here are mathematical entities based on the quantitative information used as input in the inversion. Stated differently, the probabilities are based entirely on (1) data and their uncertainties, (2) prior information as quantified here, and (3) the physical relation between data and unknown model parameters. Given these probabilities, we can calculate resolution measures, which are given by eq. (8). If $f(\mathbf{m}) = m_i$, the resolution measure is equal to the mean, $\overline{m}_i$ of the ith model parameter m_i. On the other hand, should we be interested in the covariance between the model parameters m_i and m_j, $f(\mathbf{m}) = (m_i - \overline{m}_i)(m_j - \overline{m}_j)$. In this way any estimator or estimator of dispersion can be obtained. Resolution measures usually represent the answer to questions addressing certain aspects of the subject matter in terms of a probability. For example, a question of great interest here could be formulated as follows. How likely is it, given the observed data, their uncertainties and prior information, that bulk lunar composition resembles the composition of the Earth's upper mantle?

There are a number of ways to display the results depending on the questions that we are trying to address. For the purpose of obtaining information on single parameters and their uncertainties, 1-D marginals are most appropriate. While 1-D marginal *pdf*'s are easily visualizable and provide a clear picture of the *pdf* as regards single parameters, information on any other parameters is not provided. For this, 2-D or 3-D marginal *pdf*'s are called for, as they are able to reveal the correlation that exists among several parameters. As advocated by Mosegaard & Tarantola (1995) and Tarantola (2004), we can also display a collection of models from the posterior *pdf*. Looking at, say, 100 models taken randomly from the prior and posterior *pdf* is surprisingly informative, as general features characteristic of the models, like those that are well resolved, will tend to be recurring. Displaying such a collection could be said to be our starting point, because subsequent analysis of the posterior *pdf*, in the form of uncertainties on parameters and correlations etc., is often guided by what we learn when looking at such a collection of models. Fig. 2 below shows 100 models representing the *a priori* and *a posteriori pdf* for temperature from the surface down to the CMB. These models provide us with an approximate idea of, not only, the prior information used, but also, by comparing prior and posterior, the information contained in the data. The information displayed in these movies is only a first order representation of the prior and posterior *pdf*. Increasing accuracy as concerns the *pdf* necessarily entails displaying more models. Nonetheless, what comes to mind when scrutinizing the posterior models is the variability, reflecting the inherent random nature of the MCMC method. While models are seemingly different, all of them are models with high likelihood values that predict data within uncertainties. This is highlighted in Fig. 3, where we have displayed the *a priori* and *a posteriori* data movie for a subset of the data (only mass and moment of inertia are shown here). When sampling the posterior data distribution (thick line), we immediately see how the prior random walk (thin line) is gauged when data are taken into account.

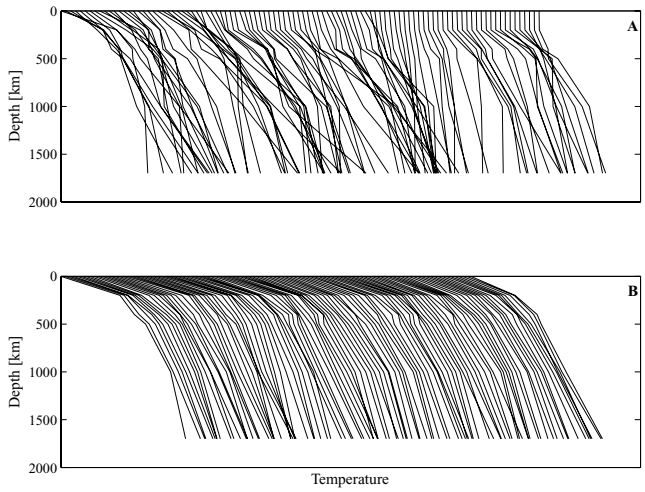

Figure 2. Collection of 100 models taken randomly from the prior (a) and posterior (b) *pdf*'s showing temperature as a function of depth. Separation between individual models is 50 °C. Comparison of prior and posterior provides a valuable insight into the information contained in the data. Prior models seem 'messy', reflecting the few prior constraints imposed on these parameters, whereas posterior models seem 'well behaved'.

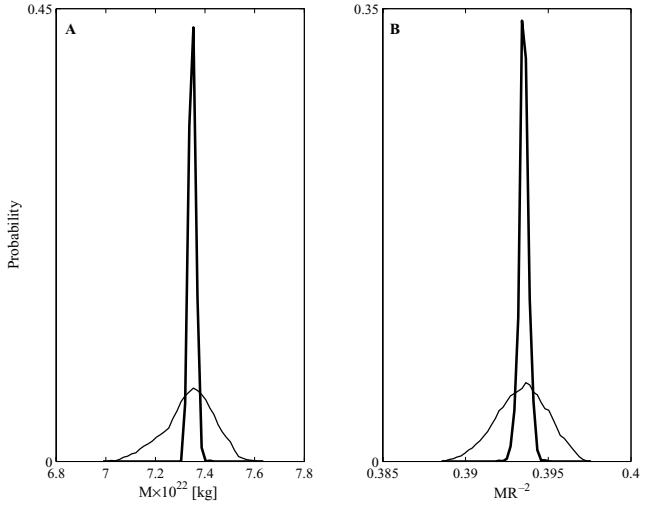

Figure 3. Prior (thin line) and posterior (thick line) data fit. The extreme narrowing of the posterior relative to the prior *pdf*'s is due to the small uncertainties on the observations. While only mass and moment of inertia are shown here, the same distributions can easily be shown for single seismic-arrival times.

5 RESULTS AND DISCUSSION

As the final results are conditioned on the nature and validity of the assumptions that go into any study, the interpretation of the results should reflect these limitations. Limitations are imposed by us, in part, because of our choice of the particular model of the Moon and the inversion method, and on us, in part, because of the nature of the data.

Chief limitations imposed by data are due to the fact that only four stations were operative, covering a small area of the front side of the moon, as well as the fact that we are confined to modelling first arrivals. Of importance in this respect, is the limited amount of data available including their quality, which limits detailed modelling and forces the assumption of radial symmetry. Because of this assumption the results are averages over the front side of the Moon, covered by the four seismic stations.

With regard to the inverse problem, we face the usual trade-off between resolution and uncertainty on estimated model parameter values, reflecting our choice of parametrization. As already pointed out, the minimum number of compositional layers was used. The resolution regarding the other parameters (ρ, v_P, v_S and T) was found on the grounds that the distribution of calculated data provided an adequate fit to the observed data distribution. Had we chosen to augment the number of layers, we would have gained in resolution, but at the same time increased the uncertainty of the estimated model parameters. It is difficult to quantify the effect of uncertainties in the thermodynamic models, however, the fact that we are confined to conditions of the terrestrial upper mantle (confining pressures at ∼150 km depth) requires only limited extrapolation of experimentally calibrated equations of state. Another factor accorded attention in the interpretation of terrestrial seismic velocities is the effect of anelasticity which causes dispersion so that the seismic-wave velocities at finite frequency ω are less than in the elastic limit ($\omega \rightarrow \infty$). Minster & Anderson (1981) consider dispersion in the low attenuation limit as given by

$$v(P, T, \omega) = v(P, T, \omega \rightarrow \infty)\left[1 - \frac{1}{2Q}\cot\left(\frac{\alpha\pi}{2}\right)\right] \qquad (14)$$

indicating that dispersion in this limit depends on pressure, temperature and frequency through their effect on the attenuation Q. Typical values of α are around 0.2–0.3, consistent with experimental results (Jackson *et al.* 2002). Due to the absence of water and volatiles, Q-values for the Moon are typically an order of magnitude higher than in the Earth (Latham *et al.* 1970). The crustal Q-value (depth range 0–45 km) is around 6000 for both P and S waves, whereas upper-mantle Q-values (depth range ∼45–560 km) are around 4000–7000 for P waves and ∼4000 for S waves and finally middle mantle Q-values (depth range ∼560–1100 km) are ∼1500 for P waves (Nakamura & Koyama 1982). Such high Q-values will result in only minor velocity changes due to anelastic effects over most of the lunar interior (<0.1 per cent). Also considering the large uncertainties in anelasticity parameters, dispersion effects will not be given further consideration here.

The primary parameters were c, T and d and Figs 4 and 5 display c for the crust and mantle in the form of 1-D prior and posterior marginals, clearly showing that c is being constrained by data. Temperature models are shown in Fig. 6 and like c, the posterior marginals for T are also seen to be significantly narrowed, signalling that inversion of seismic traveltime data are able to provide information on composition and thermal state. Our thermal profiles are generally in agreement with earlier geophysically derived selenotherms; like Huebner *et al.* (1979) and Hood & Sonett (1982) temperatures well below the solidus at a depth of 1000 km are obtained bringing us into accord with the overall seismic evidence of a solid and rigid lunar mantle (for summary discussions of these and other geophysical evidence on mantle thermal evolution and present-day state the reader is referred to e.g. Hood & Zuber 2000; Khan *et al.* 2006d). Major mineral phases and derived bulk physical properties, in the form of radial density, seismic P- and S-wave velocity profiles are shown in Figs 7–10. The remarkable homogeneity of the obtained lunar mantle mineralogy is also apparent in the resulting seismic-wave velocity profiles. Major velocity changes in the mantle are not immediately apparent, which is related to the fact that we modelled the lunar mantle using single compositions. Any transitions between upper and lower mantle arising from a change

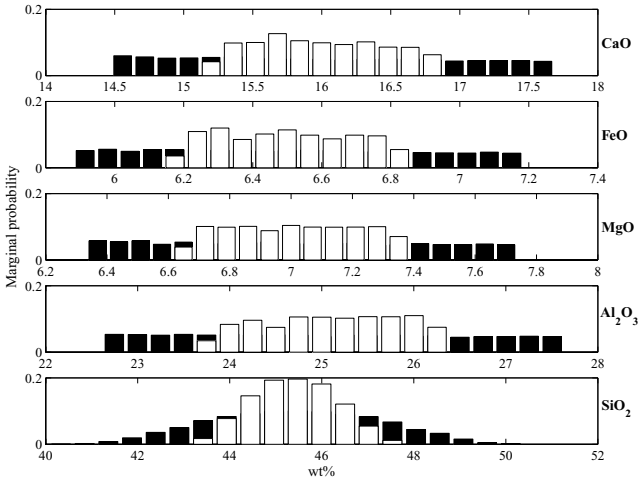

Figure 4. Prior (black bins) and posterior (white bins) marginal *pdf*'s for the oxides in the CFMAS system (marked to the right of each figure) comprising the crustal composition. The crustal composition was *a priori* bounded to lie within 5 per cent of the Taylor crustal model (see Table 5).

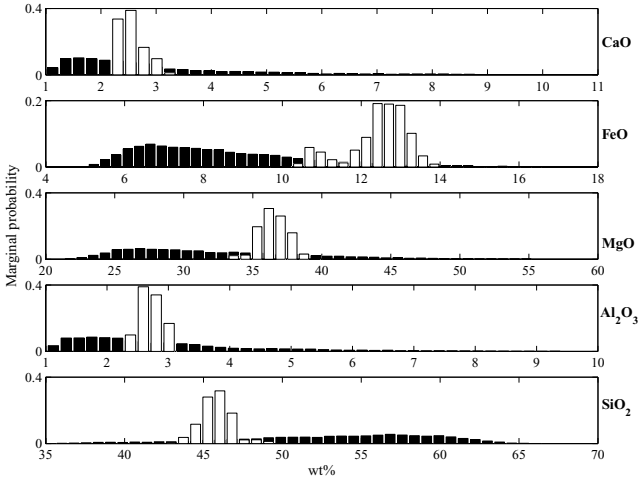

Figure 5. Prior (black bins) and posterior (white bins) marginal *pdf*'s for the oxides in the CFMAS system (marked to the right of each figure) comprising the mantle composition. *A priori* bounds on mantle composition are summarized in Table 2. Note that as we are not plotting the logarithm of the individual parameters, we do not obtain homogeneous distributions, but ones that are skewed.

in composition are thus obviously discounted, leaving only phase changes as possible markers. We searched the entire set of sampled v_P and v_S models for any velocity changes in the mantle by correlating v_P and v_S at depths of 400 and 750 km, respectively. No major velocity changes were found, reflecting the apparently remarkable homogeneity of v_P and v_S. A slight increase in density is discernible though, due to the coupled effects of pressure and increased amounts of the denser phase garnet relative to ortho and clinopyroxene. v_S is seen to decrease on going down through the mantle which is related to it being relatively more sensitive to temperature than v_P. Bulk sampled compositions and Mg#s [molar MgO/(MgO+FeO)×100] for the silicate part of the Moon are displayed in the histograms in Fig. 11. Previous bulk compositions obtained from geochemical (Taylor 1982; Warren 2005) as well as geophysical modelling (Kuskov & Kronrod 1998) and that of the Earth's upper mantle (McDonough & Sun 1995) have been included

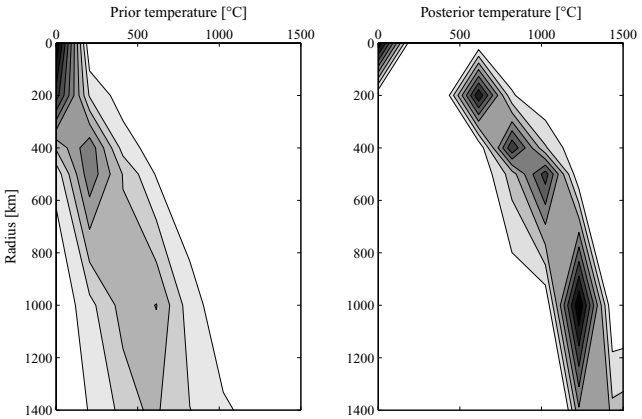

Figure 6. Marginal prior (left-hand side panel) and posterior (right-hand side panel) *pdf*'s depicting all sampled mantle selenotherms for the silicate part of the Moon, that is, from surface down to the CMB. At the six fixed depth nodes a histogram reflecting the marginal probability distribution of sampled temperature is set up. By lining up these marginals, temperature as a function of radius can be envisioned as contours directly relating their probability of occurrence. Shades of grey between white and black indicating, respectively, least and most probable outcomes. Note that the posterior *pdf*'s have not only narrowed significantly relative to the prior *pdf*'s, but that they have also been displaced. The discontinuity apparent on the posterior plot is an artefact due to the parametrization.

for comparison. Previous geophysically derived seismic velocities are compiled in Table 6 and overall agreement is seen to be present.

Concerning the core, current consensus favours a small (<1–3 per cent by volume) iron or iron core containing some light element such as S (Hood & Jones 1987; Mueller *et al.* 1988; Kuskov & Kronrod 1998; Hood *et al.* 1999; Righter 2002; Williams *et al.* 2001; Khan *et al.* 2004), in line with the prevailing model for the origin of the Moon (Canup 2004). While most geophysical and geochemical data pertaining to the lunar core seem to converge upon the necessity for a small lunar core of iron-like composition, it has to be noted that this is strictly not demanded and other compositions are also consistent with data (the reader is referred to e.g. Hood & Zuber 2000; Williams *et al.* 2001; Khan *et al.* 2004, for further discussion). The latter two studies also point to the most probable existence of small iron core with a radius of ∼350 km, in line with our results shown in Fig. 12.

Issues of obvious interest here include questions concerning convergence, stationarity, data sensitivity, model resolution and not least the trade-offs existing between the inverted parameters. Let us address the latter issue first by investigating effects of temperature changes on mantle mineralogy and physical properties as well as the associated effects of how changes in mineralogy affects physical properties (the primary parameters, c and T are distributed independently according to the prior *pdf* η_p and are thus not correlated; as we parametrized the mantle using single compositions, c and ρ, v_P and v_S are generally also uncorrelated). Fig. 13 below shows how T affects mantle mineralogy (Figs 13A–D) and the physical properties v_S (Figs 13E–H) and ρ (Figs 13I–L). At any given depth olivine content and physical properties are seen to be anticorrelated with T as expected, while ρ and v_S correlate positively with olivine content (Figs 13M–T). In general, the correlations are found to be weak and are observed to decrease as a function of depth so that they become insignificant at about 1000 km depth. Moreover, absolute values of ρ and especially v_S are seen to decrease as a function of depth, signalling that temperature effects are relatively more important than pressure effects in the Moon.

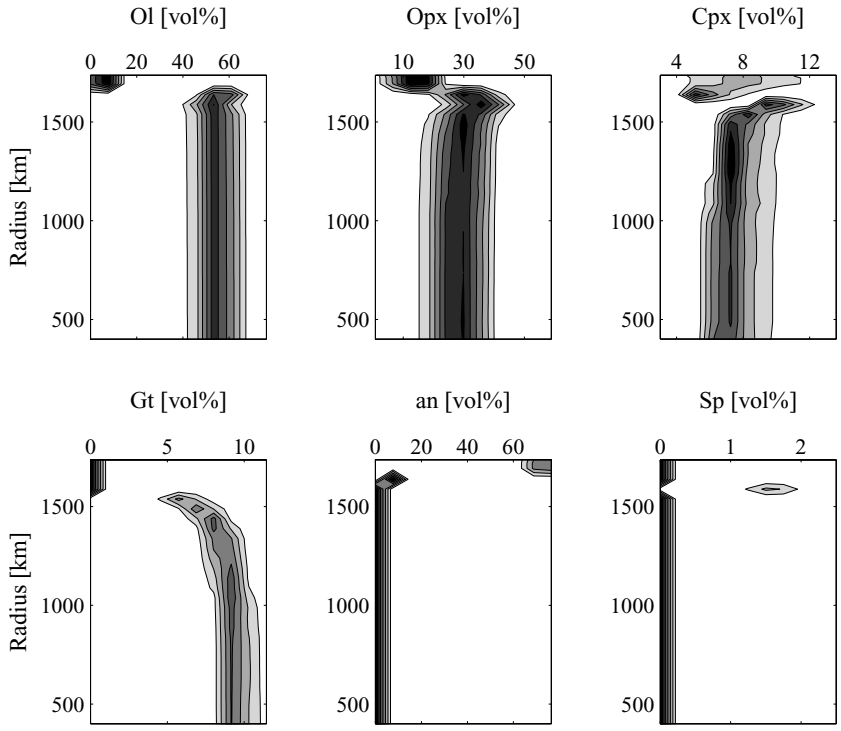

Figure 7. Marginal posterior *pdf*'s of major minerals, showing the volume per cent of each phase as a function of radius for the silicate part of the Moon. At the 31 fixed depth nodes a histogram reflecting the marginal probability distribution of sampled mineral proportions has been set up. The marginals are lined up as described in the caption of Fig. 6. Shades of grey as in Fig. 6. Abbreviations are Ol—olivine, Opx—orthopyroxene, Cpx—clinopyroxene, Gt—garnet, an—anorthite and Sp—spinel.

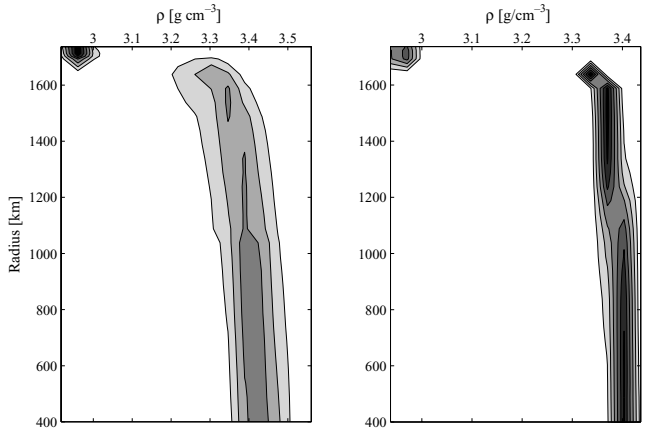

Figure 8. Marginal prior (left-hand side panel) and posterior (right-hand side panel) *pdf*'s depicting the mantle density structure for the silicate part of the Moon. The density increase in the mantle is due an increased amount of garnet. Shades of grey as in Fig. 6.

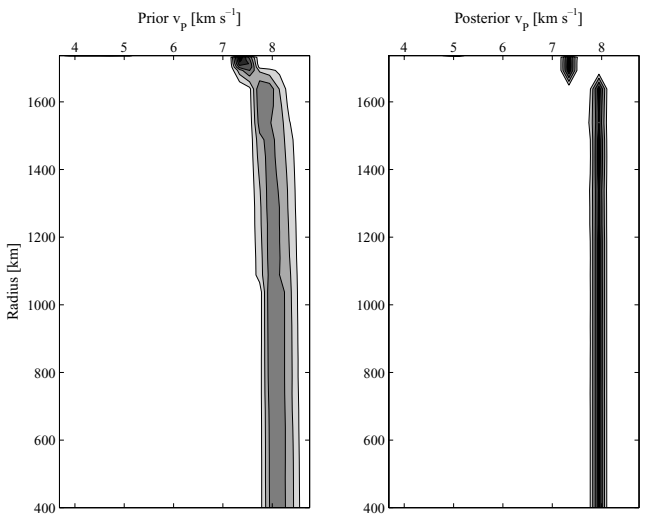

Figure 9. Marginal prior (left-hand side panel) and posterior (right-hand side panel) *pdf*'s depicting the mantle *P*-wave velocity structure for the silicate part of the Moon. Shades of grey as in Fig. 6.

Of importance when having to draw conclusions from inverse calculations, are issues of convergence and resolution. Criteria usually adopted as regards convergence, include the necessity of stabilization of inverted parameter values and similarity of these across independent chains, that is, runs, which usually provide adequate confidence in the results. Fig. 14 shows the results obtained for sampled Mg#s from the inversion of three independent posterior chains using different random number sequences. While the results vary in detail, the general characteristics are, as expected, similar.

To address the issue of data resolution, it is practical to investigate how well resolved a certain parameter is when inverting individual data sets. Fig. 14 summarizes these results, in the form of sampled Mg#s, for separate inversions of (1) only seismic data, (2) only gravity data, (3) joint inversion of all data and (4) the prior information. Inversion of individual data sets shows that while the characteristics differ among the posterior *pdf*'s, a significant narrowing of the prior *pdf* is observed, signalling that individual data sets are indeed

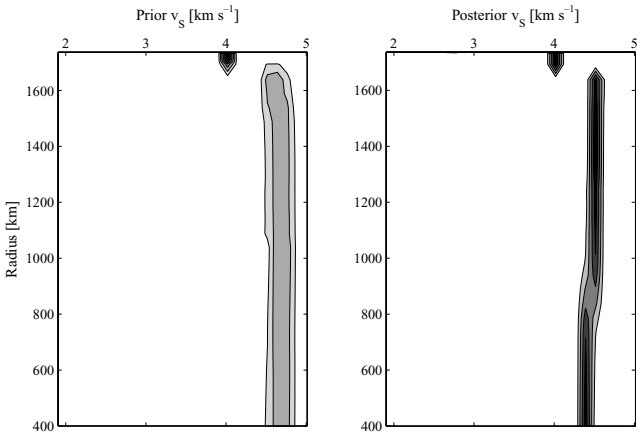

Figure 10. Marginal prior (left-hand side panel) and posterior (right-hand side panel) *pdf*'s depicting the mantle *S*-wave velocity structure for the silicate part of the Moon. The velocity decrease is related to the increased temperatures in the mantle. Shades of grey as in Fig. 6.

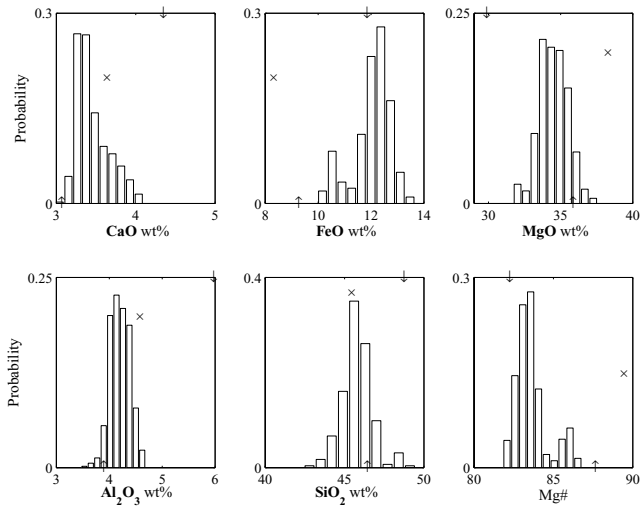

Figure 11. Marginal posterior *pdf*'s displaying bulk lunar composition and Mg# for the silicate part of the Moon (crust and mantle). Upward and downward pointing arrows indicate the bulk composition estimates of Warren (2005) and Kuskov & Kronrod (1998) (their model II), respectively, while crosses denote bulk composition of the Earth's upper mantle as estimated by McDonough & Sun (1995). In accordance with previous estimates bulk Moon is generally seen to be different from the pyrolite composition of Ringwood (1966), thought to be representative of the Earth's upper mantle.

sensitive to the inverted parameters. Moreover, the posterior *pdf* obtained by joint inversion of all data is seen to be significantly constrained when compared to those obtained by inversion of single data sets.

In having to evaluate models of lunar formation and evolution, the question of the resemblance of the lunar and terrestrial mantle composition has figured prominently (e.g. Drake 1986; Ringwood 1986; Taylor 1986; Warren 2005; Taylor *et al.* 2006). Many recent estimates of the composition of the upper mantle of the Earth (McDonough & Sun 1995; Salters & Stracke 2004) are similar to that of the pyrolite composition proposed by Ringwood (1966). These compositional estimates are principally based on studies of the composition of meteorites, mantle xenoliths and the basaltic products of mantle melting. These compositions can reproduce the seismic velocity and density profiles of the Earth's upper mantle for likely geotherms (Murakami & Yoshioka 2001). Moreover, they also have a sufficiently high Mg#, close to 90, to generate melts with a Mg# resembling the most primitive mid-ocean ridge basalts. The results of our inversion procedure generate mantle compositions for the Moon that are strikingly different to that of pyrolite, with our models having somewhat lower SiO_2 and MgO than the pyrolite composition. Almost all of our models have higher FeO than pyrolite, and somewhat lower CaO and Al_2O_3 contents. Our results, therefore, indicate that the mantle composition of the Moon is different from that of the Earth's. Our estimates of bulk lunar composition (silicate portion of the Moon) obtained here, lends additional support to this contention. The discrepancy is further exemplified by the Mg#, where we find a bulk lunar Mg# of approximately 82 and our range of values match the observed Mg# of the most primitive mare basalts. Moreover, as we consistently found bulk lunar Mg# differing significantly from that of the Earth's (89), we believe that this compositional difference is robust, and that it reflects not only a different origin, but also different evolutionary histories for the Earth and Moon. Giant impact scenarios, originally proposed by Hartmann & Davis (1975) and Cameron & Ward (1976), where the Moon forms from the silicate debris that comes to lie in a circumterrestrial ring have done away with most of the geochemical obstacles. As most of the material (>80 per cent, Canup 2004) making up the Moon is derived from the mantle of the impactor any present-day Earth–Moon differences are most easily explained, at least to first order, as originating from the distinct chemical makeup of the impactor.

Table 6. Seismic *P*- and *S*-wave velocities obtained from earlier studies. The results by Nakamura, Khan *et al.* and Lognonné *et al.* were obtained by inversion of lunar seismic-arrival times, whereas the study by Kuskov *et al.* represents results obtained from an inversion of the velocity model derived by Nakamura. Whereas the former three investigations inverted for 1-D velocity profiles, Kuskov *et al.* inverted the Nakamura velocity profiles to constrain composition.

Model	v_P (km s^{-1})	v_S (km s^{-1})
Kuskov *et al.* (2002)		
Upper mantle (60–500 km)	7.4–8.2	4.2–4.7
Lower mantle (5000–1000 km)	7.6–8.4	4.2–4.6
Nakamura (1983)		
Upper mantle (270–500 km)	7.46 ± 0.25	4.25 ± 0.1
Lower mantle (500–1000 km)	8.26 ± 0.4	4.65 ± 0.16
Khan *et al.* (2000)		
Upper mantle (45–500 km)	8.0 ± 0.8	4.0 ± 0.9
Lower mantle (700–800 km)	9.0 ± 1.9	5.5 ± 0.9
Lognonné *et al.* (2003)		
Upper mantle (300–500 km)	7.75 ± 0.15	4.4 ± 0.15
Lower mantle (500–750 km)	7.9 ± 0.3	4.2 ± 0.3

6 CONCLUSION

As outlined in Fig. 1, the method presented here is a general approach to an integrated inversion of *a priori* unrelated geophysical data to constrain composition, thermal state and other parameters pertinent to the specific problem being treated. Traditionally, geophysical data are inverted for parameters that are a physical manifestation of those data, for example, inversion of seismic data for seismic-wave velocities, inversion of gravity data for density structure, electromagnetic sounding data for electrical conductivity structure etc. However, in the absence of physical laws or laboratory measurements

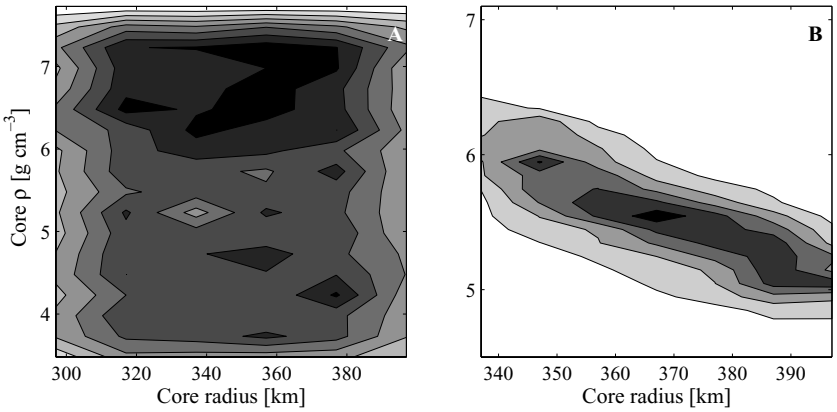

Figure 12. Prior (a) and posterior (b) marginal 2-D *pdf*'s showing sampled core densities and sizes. Data seem to favour densities indicative of Fe 10 wt. per cent S cores with a most probable radius around 340 km in line with earlier inferences (see main text for further discussion). The measured values for Fe 10 wt. per cent S at 1500 °C and 5 GPa is 5.7 g cm^{-3} (Sanloup *et al.* 2000).

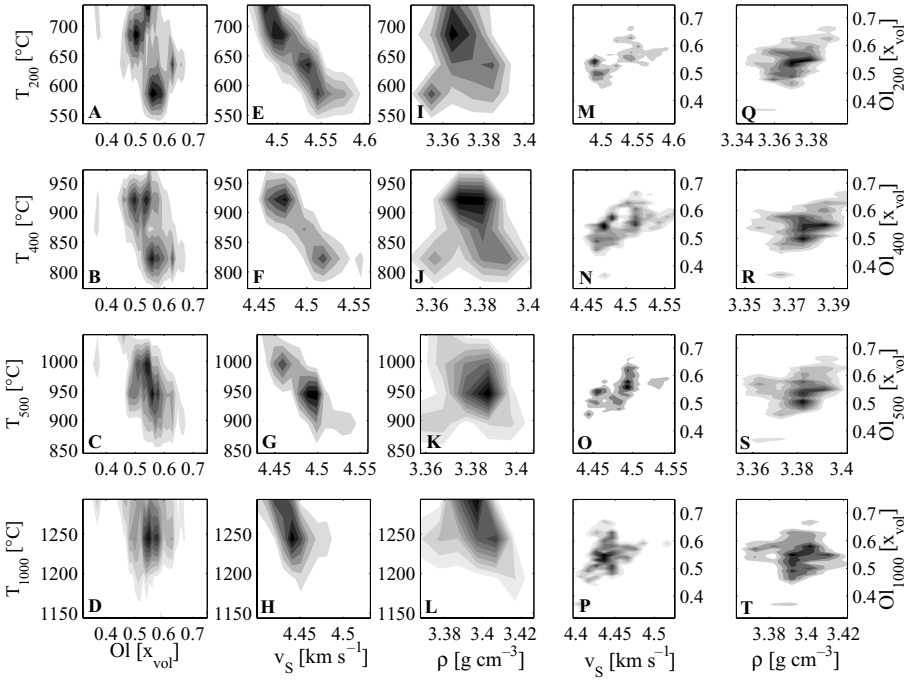

Figure 13. Plots showing the correlation between several sampled parameters at various depths (indicated as subscripts on the *y*-axes). (A–D) T versus Ol content, (E–H) T versus v_S, (I–L) T versus ρ, (M–P) Ol content versus v_S and (Q–T) Ol content versus ρ. Olivine is given in volume fractions ($x_{\rm vol}$) and shades of grey as before.

correlating, for example, seismic-wave velocities and electrical conductivities there is no obvious way of constraining the electrical conductivity structure from an inversion of seismic-arrival times. Therefore, inverting for a set of parameters which describe the system being studied at a fundamental level, that is, chemical composition and temperature, rather than density and seismic-wave velocity, allows us to naturally link geophysical data that are not *a priori* related. The generality of the method makes it easily extendable so as to include more complex chemical models and other kinds of geophysical data in the inversion.

We used a probabilistic inference approach to combine the information describing the various geochemical and geophysical aspects of the problem. This was specifically done by introducing a joint posterior *pdf* which considers not only a suite of properties (chemical composition, temperature, layer thickness, etc.), but also multiple types of geophysical data. In the present formulation, we partitioned the model parameter space into a primary and secondary model parameter space, according to fundamental and geophysical parameters and employed a joint prior *pdf* to describe this information. The joint prior *pdf* was written as the product of a prior *pdf* over primary parameters and a conditional prior *pdf* over secondary parameters. The joint likelihood function was given as the product of the likelihood functions for each individual data set. The generality of the present formulation makes it easily extendable to include other kinds of geophysical data as well as forward modelling sequences.

As regards sampling models from the joint posterior *pdf*, we used a stochastically based sampling algorithm. Specifically, this was done by using a MCMC sampling algorithm, that is, by performing a random walk in a multidimensional model space that combines

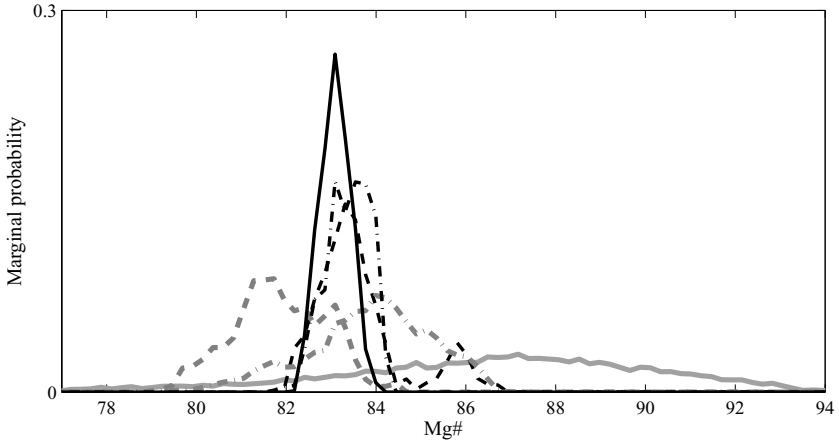

Figure 14. Marginal prior and several posterior *pdf*'s showing sampled bulk lunar Mg#s for the silicate part of the Moon, obtained from an inversion of prior information (grey line), only gravity data (grey dot–dashed line), only seismic data (grey-dashed line), all data jointly (dashed line), all data jointly with different random seeds (full and dot–dashed line), respectively. Resolution is seen to increase as we add information in the inversion.

prior information with information from measurements and from the theoretical relationship between data and model parameters. Input to the algorithm were random models generated according to the (1) primary prior *pdf* , (2) the generalization to the joint model space, by sampling the secondary prior *pdf* (conditional to primary parameters) and (3) a modification of the joint prior random walk by considering the likelihood function to sample the joint posterior *pdf* using the Metropolis rule. As output we assimilated random realizations of the posterior *pdf* , which contain all the information about our parametrized physical system.

ACKNOWLEDGMENTS

The manuscript benefited from two anonymous reviews. Comments by Y. Nakamura and S. R. Taylor on an earlier version of this manuscript are also appreciated. AK gratefully acknowledges support from the Carlsberg foundation and the financial support provided through the European Community's Improving Human Potential Programme under contract RTN2-2001-00414, MAGE. JM would like to thank NERC for funding (fellowship NER/I/S/2002/00609/2).

REFERENCES

Besag, J., Green, P., Higdon, D. & Mengersen, K., 1995. Bayesian computation and stochastic systems, *Stat. Sci.,* **10,** 3.

Bosch, M., 1999. Lithologic tomography: From plural geophysical data to lithology estimation, *J. geophys. Res.,* **104,** 749.

Bulow, R.C., Johnson, C.L. & Shearer, P.M., 2005. New events discovered in the Apollo lunar seismic data, *J. geophys. Res.,* **110,** E10003, doi:10.1029/2005JE002414.

Cameron, A.G.W. & Ward, W.R., 1976. The origin of the Moon, in *Lunar Planet. Sci. Conf. VII, Abstract*, Vol. 120, LPI, Houston.

Cammarano, F., Goes, S., Vacher, P. & Giardini, D., 2003. Inferring upper mantle temperatures from seismic velocities, *Phys. Earth planet. Inter.,* **138,** 197.

Canup, R.M., 2004. Simulations of a late lunar-forming impact, *Icarus,* **168,** 433.

Connolly, J.A.D., 2005. Computation of phase equilibria by linear programming: a tool for geodynamic modeling and an application to subduction zone decarbonation, *Earth planet. Sci. Lett.,* **236,** 524.

Connolly, J.A.D. & Kerrick, D.M., 2002. Metamorphic controls on seismic velocity of subducted oceanic crust at 100–250 km depth. *Earth planet. Sci. Lett.,* **204,** 61.

Cooper, M. & Kovach, R.L., 1974. Lunar near surface structure, *Rev. Geophys. Space Phys.,* **12,** 291.

Deschamps, F. & Trampert, J., 2004. Towards a lower mantle reference temperature and composition, *Earth planet. Sci. Lett.,* **222,** 161.

Drake, M.J., 1986. Is lunar bulk material similar to Earth's mantle? In *Origin of the Moon*, Vol. 105, eds Hartmann, W.K., Phillips, R.J. & Taylor, G.J., LPI, Houston.

Gelfand, A.E. & Smith, A.F.M., 1990. Sampling based-approaches to calculating marginal densities, *J. Am. Stat. Assoc.,* **85,** 398.

Gelman, A. & Rubin, D.B., 1992. Inference from iterative simulation using multiple sequences, *Stat. Sci.,* **7,** 457.

Goes, S., Govers, R. & Vacher, P., 2000. Shallow mantle temperatures under Europe from *P* and *S* wave tomography, *J. geophys. Res.,* **105,** 11 153.

Godey, S., Deschamps, F., Trampert, J. & Snieder, R., 2004. Thermal and compositional anomalies beneath the North American continent, *J. geophys. Res.,* **109,** B01308, doi:10.1029/2002JB002263.

Goins, N.R., Dainty, A. & Toksöz, M.N., 1981a. Lunar Seismology: The Internal Structure of the Moon, *J. geophys. Res.,* **86,** 5061.

Goins, N., Dainty, A. & Toksöz, M.N., 1981b. Seismic Energy Release of the Moon, *J. geophys. Res.,* **86,** 378.

Hartmann, W.K. & Davis, D.R., 1975. Satellite-sized planetesimals and lunar origin, *Icarus,* **24,** 504.

Hastings, W.K., 1970. Monte Carlo sampling methods using Markov chains and their applications, *Biometrika,* **57,** 97.

Hirschmann, M., 2000. Mantle solidus: Experimental constraints and the effects of peridotite composition, *Geochem. Geophys. Geosyst.,* **1**(10), doi:10.1029/2000GC000070.

Holland, T.J.B. & Powell, R., 1996. Thermodynamics of order-disorder in minerals. 2. Symmetric formalism applied to solid solutions, *Am. Min.,* **81,** 1425.

Holland, T.J.B. & Powell, R., 1998. An internally consistent thermodynamic data set for phases of petrological interest, *J. Met. Geol.,* **16,** 309.

Hons, M.S. & Hildebrand, A.R., 2004. Compressional and shear wave velocities in meteorites, *Lunar Planet Sci. Conf. 35th, Abstract,* Vol. 2059.

Hood, L.L. & Sonett, C.P., 1982. Limits on the lunar temperature profile, *Geophys. Res. Lett.,* **9,** 37.

Hood, L.L. & Jones, J.H., 1987. geophysical constraints on lunar bulk composition and structure: a reassessment, *J. geophys. Res.,* **92,** 396.

Hood, L.L., Mitchell, D.L., Lin, R.P., Acuna, M.H. & Binder, A.B., 1999. Initial measurements of the lunar-induced magnetic dipole moment using lunar prospector magnetometer data, *Geophys. Res. Lett.,* **26,** 2327.

Hood, L.L. & Zuber, M.T., 2000. Recent refinements in geophysical constraints on lunar origin and evolution, in *Origin of the Earth and Moon.*

Huebner, J.S., Wiggins, L.B. & Duba, A.G., 1979. Electrical conductivity of pyroxene which contains trivalent cations—laboratory measurements and the lunar temperature profile, *J. geophys. Res.,* **84,** 4652.

Jackson, I., Gerald, J.D.F., Faul, U.H. & Tan, B.H., 2002. Grain size-sensitive seismic wave attenuation in polycrystalline olivine, *J. geophys. Res.,* **107,** 2002, doi:10.1029/2001JB001225.

Kanamori, H., Nur, A., Chung, D.H. & Simmons, G., 1970. Elastic wave velocities of lunar samples at high pressures and their geophysical implications, *Geochim. Cosmochim. Acta, suppl.,* Vol. 1, Proc. of the Apollo 11 Lunar Science Conference, 2289.

Khan, A., Mosegaard, K. & Rasmussen, K.L., 2000. A new seismic velocity model for the Moon from a Monte Carlo inversion of the Apollo lunar seismic data, *Geophys. Res. Lett.,* **27,** 1591.

Khan, A. & Mosegaard, K., 2002. An inquiry into the lunar interior: a nonlinear inversion of the apollo lunar seismic data, *J. geophys. Res.,* **107**(E6), doi10.1029/2001JE001658.

Khan, A., Mosegaard, K., Williams, J.G. & Lognonné, P., 2004. Does the Moon possess a molten core? Probing the deep lunar interior using results from LLR and lunar prospector, *J. geophys. Res.,* **109** (E09007), doi:10.1029/2004JE002294.

Khan, A., Connolly, J.A.D. & Olsen, N., 2006a. Constraining the composition and thermal state of the mantle beneath Europe from inversion of long-period electromagnetic sounding data, *J. geophys. Res.*, in press.

Khan, A., Connolly, J.A.D., Olsen, N. & Mosegaard, K., 2006b. Constraining the composition and thermal state of the Moon from an inversion of lunar day-side transfer functions, *Earth planet. Sci. Lett.,* **248,** doi:10.1016/j.epsl.2006.04.008.

Khan, A. & Connolly, J.A.D., 2006. Constraining the composition and thermal state of Mars from an inversion of geophysical data, *Earth planet. Sci. Lett.*, in press.

Khan, A., Maclennan, J., Connolly, J.A.D. & Taylor, S.R., 2006d. Are the Earth and the Moon compositionally alike?—Inferences on lunar composition and implications for lunar origin and evolution from geophysical modeling. *J. geophys. Res.,* **111** (E05005), doi:10.1029/2005JE002608.

Konopliv, A., Binder, A.B., Hood, L.L., Kucinskas, A.B., Sjögren, W.L. & Williams, J.G., 1998. Improved Gravity Field of the Moon From Lunar Prospector, *Science,* **281,** 1476.

Kovach, R.L. & Watkins, J., 1973. Apollo 17 seismic profiling—Probing the lunar crust, *Science,* **180,** 1063.

Kuskov, O.L. & Kronrod, V.A., 1998. Constitution of the Moon: 5. Constraints on density, temperature and radius of a core, *Phys. Earth planet. Inter.,* **107,** 285.

Kuskov, O.L. & Kronrod, V.A., 2001. Core sizes and internal structure of Earth's and Jupiter's satellites, *Icarus,* **151,** 204.

Kuskov, O.L. & Kronrod, V.A., 2005. Internal structure of Europa and Callisto, *Icarus,* **177,** 550.

Kuskov, O.L., Kronrod, V.A. & Hood, L.L., 2002. Geochemical constraints on the seismic properties of the lunar mantle, *Phys. Earth planet. Inter.,* **134,** 175.

Latham, G.V., Ewing, M., Press, F. & Sutton, G., 1969. Apollo passive seismic experiment, *Science,* **165,** 241.

Latham, G.V. *et al.*, 1970. Passive seismic experiment, *Science,* **167,** 455.

Latham, G.V. *et al.*, 1972. Passive Seismic Experiment, in *Apollo 16 Preliminary Science Report, NASA SP-315*, Sec. 9, 29 pp

Lognonné, P., Gagnepain-Beyneix, J. & Chenet, H., 2003. A New Seismic Model of the Moon: Implications for Structure, Thermal Evolution and Formation of the Moon, *Earth planet. Sci. Lett.,* **211,** 27.

Mattern, E., Matas, J., Ricard, Y. & Bass, J., 2005. Lower mantle composition and temperature from mineral physics and thermodynamic modeling, *Geophys. J. Int.,* **160,** 973.

McDonough, W.F. & Sun, S.S., 1995. The composition of the Earth, *Chem. Geol.,* **120** (3–4), 223.

Metropolis, N., Rosenbluth, A.W., Rosenbluth, M.N., Teller, A.H. & Teller, E., 1953. Equation of state calculations by fast computing machines, *J. Chem. Phys.,* **21,** 1087.

Minster, J.B. & Anderson, D.L., 1981. A model of dislocation-controlled rheology for the mantle, *Phil. Trans. R. Soc. London,* **299,** 319.

Mosegaard, K., 1998. Resolution analysis of general inverse problems through inverse Monte Carlo sampling, *Inverse Problems,* **14,** 405.

Mosegaard, K. & Tarantola, A., 1995. Monte Carlo sampling of solutions to inverse problems, *J. geophys. Res.,* **100,** 12431.

Mosegaard, K. & Tarantola, A., 2002. Probabilistic approach to inverse problems, in *International Handbook of Earthquake and Engineering Seismology*, p. 237, Academic Press, New York.

Mosegaard, K. & Sambridge, M., 2002. Monte Carlo analysis of inverse problems, *Inverse Problems,* **18,** 29.

Mueller, S., Taylor, G.J. & Phillips, R.J., 1988. Lunar composition: a geophysical and petrological synthesis, *J. geophys. Res.,* **93,** 6338.

Murakami, T. & Yoshioka, S., 2001. The relationship between the physical properties of the assumed pyrolite composition and depth distributions of seismic velocities in the upper mantle, *Phys. Earth planet. Inter.,* **125,** 1.

Nakamura, Y., 1980. Shallow moonquakes: how they compare with earthquakes, *Proc. Lunar Sci. Conf. 11th*, 1847.

Nakamura, Y., 1983. Seismic velocity structure of the lunar mantle, *J. geophys. Res.,* **88,** 677.

Nakamura, Y., 2005. Farside deep moonquakes and deep interior of the Moon, *J. geophys. Res.,* **110,** E)1001, doi:10.1029/2004JE002332.

Nakamura, Y., Latham, G.V. & Dorman, J., 1980. How we processed Apollo lunar seismic data, *Phys. Earth planet. Inter.,* **21,** 218.

Nakamura, Y., Dorman, J., Duennebier, R., Ewing, M., Lammlein, D. & Latham, G.V., 1974a. High-frequency lunar teleseismic events, *Proc. Lunar Sci. Conf. 5th*, 2883.

Nakamura, Y., Latham, G.V., Dorman, J. & Harris, J., 1981. Passive Seismic Experiment Long-Period Event Catalog, Final Version, 1969 day 202–1977 day 273, 314 pp., Galveston Geophysics Laboratory Contribution No. 491, University of Texas, Austin.

Nakamura, Y. & Koyama, J., 1982. Seismic Q of the lunar upper mantle, *J. geophys. Res.,* **(87),** 4855.

Nakamura, Y., Latham, G.V. & Dorman, J., 1982. Apollo Lunar Seismic Experiment-Final Summary, *J. geophys. Res.,* **87,** A117.

Righter, K., 2002. Does the moon have a metallic core? Constraints from giant-impact modelling and siderophile elements, *Icarus,* **158,** 1.

Ringwood, A.E., 1966. Mineralogy of the mantle, in *Advances in Earth Science*, p. 357, ed. Hurley, P., MIT Press, Boston.

Ringwood, A.E., 1986. Composition and origin of the Moon, in *Origin of the Moon*, p. 673, eds Hartmann, W.K., Phillips, R.J. & Taylor, G.J., LPI, Houston.

Rubie, D.C. & Thompson, A.B., 1985. Kinetics of metamorphic reactions, in *Metamorphic Reactions: Kinetics, Textures and Deformation*, p. 291, eds Thompson, A.B. & Rubie, D.C., Springer, New York.

Salters, V.J.M. & Stracke, A., 2004. Composition of the depleted mantle, *Geochim. Geophys. Geosyst.,* **5,** art. no. Q05004.

Sambridge, M. & Mosegaard, K., 2002. Monte Carlo methods in geophysical inverse problems, *Rev. Geophys.,* **40**(3), doi:10.1029/2000RG000089.

Sanloup, C., Guyot, F., Gillet, P., Fiquet, G., Mezouar, M. & Martinez, I., 2000. Density measurements of liquid Fe-S alloys at high-pressure, *Geophys. Res. Lett.,* **27,** 811.

Shapiro, N.M. & Ritzwoller, M.H., 2004. Thermodynamic constraints on seismic inversions, *Geophys. J. Int.,* **157,** 1175.

Smith, D.E., Zuber, M.T., Neumann, G.A. & Lemoine, F.G., 1997. Topography of the Moon from the Clementine LIDAR, *J. geophys. Res.,* **102,** 1591.

Tarantola, A., 2004. *Inverse Problem Theory and Methods for Model Parameter Estimation*, SIAM, Philadelphia.

Tarantola, A. & Valette, B., 1982. Inverse problems: Quest for information, *J. Geophys.,* **50,** 159.

Taylor, L.A., Taylor, G.J. & Taylor, S.R., 2006. The Moon: A. Taylor perspective, *Geochim. Cosmochim: Acta,* in press.

Taylor, S.R., 1982. *Planetary Science: A Lunar Perspective*, LPI, Houston.

Taylor, S.R., 1986. The origin of the Moon—Geochemical considerations, in *Origin of the Moon*, p. 125, eds Hartmann, W.K., Phillips, R.J. & Taylor, G.J., LPI, Houston.

Tierney, L., 1994. Markov chains for exploring posterior distributions, *Ann. Stat.,* **22,** 1701.

Toksöz, M.N., 1974. Geophysical data and the interior of the Moon, *Ann. Rev. Earth planet. Sci.,* **2,** 151.

Toksöz, M.N., Dainty, A.M., Solomon, S.C. & Anderson, K.R., 1974. Structure of the Moon, *Rev. Geophys.,* **12,** 539.

Trampert, J., Deschamps, F., Resovsky, J. & D. Yuen, 2004. Chemical heterogeneities throughout the lower mantle, *Science,* **306,** 853.

Yomogida, K. & Matsui, T., 1983. Physical properties of ordinary chondrites, *J. geophys. Res.,* **88,** 9513.

Warren, P., 2005. 'New' lunar meteorites: II. Implications for composition of the global lunar surface, lunar crust, and the bulk Moon, *Met. planet. Sci.,* **40,** 1.

Watt, J.P., Davies, G.F. & O'Connell, R.J., 1976. The elastic properties of composite minerals, *Rev. Geophys. Space Phys.,* **14,** 541.

Williams, J.G., Boggs, D.H., Yoder, C.F., Radcliff, J.T. & Dickey, J.O., 2001. Lunar rotational dissipation in solid body and molten core, *J. geophys. Res.,* **106,** 27 933.

Wood, B.J. & Holloway, J.R., 1984. A thermodynamic model for subsolidus equilibria in the system CaO-MgO-Al2O_3-SiO_2, *Geochim. Cosmochim. Acta,* **66,** 159.

Xu, Y.S., Shankland, T.J. & Poe, B.T., 2000. Laboratory- based electrical conductivity in the Earth's mantle, *J. geophys. Res.,* **108,** 2314.